RAPID SIMULATIONS OF PURE SWAY MOTION USING FVM IN OpenFOAM

Vuko Vukčević (Faculty of Mechanical Engineering and Naval Architecture, Croatia)
Anders Östman (MARINTEK, Norway)
Hrvoje Jasak (Wikki Ltd, United Kingdom)
(Faculty of Mechanical Engineering and Naval Architecture, Croatia)

1 SUMMARY

The paper describes simulation results for pure sway motions for DTMB 5415 US Navy combatant and MOERI container ship (KCS) hulls. Finite Volume Method (FVM) on unstructured polyhedral grids with local refinement zones is used. Free surface is modelled using the Volume-of-Fluid (VOF) interface capturing approach, while the thickness of the transitional region is controlled via new formulation of the compressive term in the VOF transport equation. Two-equation $k-\omega$ SST turbulence model is used for all simulations. Mesh motion is modelled as a rigid body motion, moving the cells at each time step and updating the convective mesh flux. The method has been implemented in foam-extend, a fork of the open source software OpenFOAM [13].

2 INTRODUCTION

Computational Fluid Dynamics (CFD) is currently gaining attention in the marine industry. For this reason, a growing effort to validate CFD codes is under way [6], both for steady resistance and various transient calculations: wave diffraction, sea-keeping, manoeuvring and others. In this article, we shall present an attempt to efficiently model pure sway motion. Although extension to pure yaw motion and combined sway/yaw are straightforward, such simulations are not presented in this work.
Pure sway simulations of DTMB 5415 and KCS at fixed even keel are presented, comparing dimensionless hydrodynamic forces and moments with experimental results. Additionally, three different Courant-Friedrichs-Lewy (CFL) numbers were used for the KCS case. Mesh details and CPU times are reported for all simulations.

3 APPROACH

In this section the mathematical model used in this work will be presented. Second-order accurate FVM is used to discretize the equations [4].

3.1 Mathematical model

The mathematical model presented in this work is based on the Navier- Stokes equations where the free surface is captured using the VOF approach [11]. Turbulence is modelled with the $k-\omega$ SST two-equation model [8], [9]. The following governing equations are of mixture type, i.e. all fields are defined in both phases an are assumed continuous across the interface:

- Density, ρ, viscosity, ν and velocity $\mathbf{u}$ of the mixture are defined from following algebraic expressions that assume linear variation with α:

$$\rho = \alpha\rho_1 + (1-\alpha)\rho_2\,, \tag{1}$$

$$\mu = \alpha\mu_1 + (1-\alpha)\mu_2\,, \tag{2}$$

$$\mathbf{u} = \alpha\mathbf{u}_1 + (1-\alpha)\mathbf{u}_2\,. \tag{3}$$

- Volumetric continuity equation:

$$\nabla\bullet\mathbf{u} = 0\,. \tag{4}$$

  Phase continuity will follow from the α equation (8) for $\alpha = \{0, 1\}$.

- We first consider the mixture momentum equation at rest which gives a balance of the static pressure and volumetric body force, such that $p = \rho\mathbf{g}\bullet\mathbf{x}$, coming from $\nabla p = \rho\mathbf{g}$. For numerical reasons, volumetric body force is problematic since it is represented by the $\rho\mathbf{g}$ source term in the momentum equation. Hence, it needs to be reformulated as the flux term for numerical consistency. This will give identical support stencil to the terms in balance and is achieved by decomposing the pressure into hydrostatic ($\rho\mathbf{g}\bullet\mathbf{x}$) and dynamic ($p_d$) part:

$$p = p_d + \rho\mathbf{g}\bullet\mathbf{x}\,, \tag{5}$$

where $\mathbf{g}$ is the gravitational acceleration vector and $\mathbf{x}$ is the position vector. Inserting (5) into the term pairing, results in:

$$-\nabla p + \rho\mathbf{g} = -\nabla p_d - (\mathbf{g}\bullet\mathbf{x}\nabla\rho)\,. \tag{6}$$

The pressure equation is then formulated from equation (4) in terms of p_d, where p can be reconstructed using (5). Finally, mixture momentum equation for the two-phase system reads:

$$\begin{aligned}&\frac{\partial(\rho\mathbf{u})}{\partial t} + \nabla\bullet(\rho(\mathbf{u}-\mathbf{u}_M)\mathbf{u})\\ &= \nabla\bullet\sigma_{eff} - \nabla p_d - (\mathbf{g}\bullet\mathbf{x}\nabla\rho)\,,\end{aligned} \tag{7}$$

where $\mathbf{u}_M$ denotes velocity field due to mesh motion [2]. Since the mesh is moving as a rigid body, $\mathbf{u}_M$ is equal to the planar motion mechanism (PMM) velocity at a given time instant. σ_{eff} captures the effects of both laminar viscosity and turbulent Reynlods stress along with additional terms arising from two-phase model [1], [11].

- Phase continuity equation defined in terms of volume fraction α, derived from phase mass conservation:

$$\frac{\partial\alpha}{\partial t} + \nabla\bullet((\mathbf{u}-\mathbf{u}_M)\alpha) + \nabla\bullet(\mathbf{u}_r\alpha(1-\alpha)) = 0\,, \tag{8}$$

where the last term resulting from the two-phase formulation is reformulated to preserve a sharp interface [10]. The term is active only in the vicinity of the free surface due to the $\alpha(1-\alpha)$ prefactor that vanishes for $\alpha = \{0, 1\}$. $\mathbf{u}_r$ is the relative velocity field that is oriented towards the free surface in the normal direction. In [10], $\mathbf{u}_r$ is flow dependent: it is scaled based on the flux through the interface, whereas in the novel approach introduced in this study it is treated as a numerical parameter which compresses the interface to prevent excessive diffusion:

$$\mathbf{u}_r = c_\alpha\hat{\mathbf{n}}_\Gamma\frac{CFL_{ref}\Delta x}{\Delta t}\,, \tag{9}$$

where c_α is the compression constant which controls the sharpness of the interface (usually taken as one) and $\hat{\mathbf{n}}_\Gamma$ is the vector normal to the free surface. $CFL_{ref} = 0.5$ is the reference compression CFL number, Δt denotes the time step size and Δx stands for the distance between cell centres sharing an internal face. This formulation is independent of the physical flux through the interface, making the compression a purely numerical parameter which can be tuned to obtain desired sharpness of the interface.

- $k-\omega$ SST model which takes into account the change of fluid properties across the interface reads:

$$\begin{aligned}&\frac{\partial(\rho\omega)}{\partial t} + \nabla\bullet(\rho(\mathbf{u}-\mathbf{u}_M)\omega) - \nabla\bullet(\rho D_{\omega eff}\nabla\omega)\\ &= \rho\left(\gamma S^2 - \beta\omega^2 + 2(1-F_1)\frac{\sigma_{\omega 2}}{\omega}\nabla k\bullet\nabla\omega\right)\,,\end{aligned}$$

$$\begin{aligned}&\frac{\partial(\rho k)}{\partial t} + \nabla\bullet(\rho(\mathbf{u}-\mathbf{u}_M)k) - \nabla\bullet(\rho D_{\omega eff}\nabla k)\\ &= \rho\left(P_k - \beta^* k\omega\right)\,.\end{aligned} \tag{10}$$

When specific dissipation and turbulent kinetic energy are obtained, one can update the turbulent dynamic viscosity with algebraic expression:

$$\nu_T = \frac{a_1 k}{\max(a_1\omega, SF_2)}\,. \tag{11}$$

The model is used with wall functions.

3.2 Numerical procedure

Finite Volume Method with support for arbitrary polyhedral control volumes is used in this work [4]. The above equations are solved in integral, strongly conservative form. Surface integrals resulting from diffusive transport are approximated using linear interpolation with non-orthogonal correction. The convective terms are discretized with a second order linear upwind scheme for momentum and van Leer's Total Variation Diminishing (TVD) [12] scheme for the volume fraction. For compressive term in (4), α is interpolated using novel VOF compression scheme which smoothly varies from linear interpolation when $\alpha \approx 0.5$ to upwind when α is close to 0 or 1. Hence, second order accuracy in space is achieved. Details on general discretization and solution methods can be found in [4], [3]. Segregated solution algorithm based on combination of SIMPLE and PISO algorithms is used. In this work, momentum and volume fraction equations are solved twice in each time step leading to two SIMPLE correctors. Pressure equation is solved four times per one SIMPLE corrector. This is needed in order to properly resolve $\alpha - \mathbf{u} - p_d$ coupling. Implicit treatment of all governing equations allows maximum CFL numbers to be greater than one. In this work, typical maximum CFL number was 50 to 500.

4 TEST CASES

The presented algorithm is used for two similar simulations with different geometry. Both simulations

are concerned with pure sway motion of a ship with forward speed, i.e. fixed carriage velocity. Fixed even keel conditions are used and the hydrodynamic forces and moments on the ship's hull are calculated and reduced to their dimensionless form according to the guidelines provided in [7]. The first simulation is a bare hull, DTMB 5415 US Navy combatant with bilge keels where the forces and moments are compared with [14]. The second case presents the MOERI container ship (KCS) with rudder only. Even though the self-propulsion is considered in the experiments regarding KCS, propeller was not modelled in this study. Since the experiment reported carriage velocity with maximum variation of 0.05% relative to mean value, the approach taken here could be justified. For reference, reader is referred to [7]. In order to reduce the transitional effects in the beginning, both simulations are initialised with the rapid steady state solution described in [5]. Hence, forward motion is modelled by prescribing fixed inlet velocity, while the pure sway motion is accounted for via rigid body mesh motion.

4.1 DTMB 5415 US Navy combatant

Pure sway motion of a DTMB 5415 US Navy combatant model with bilge keels is simulated. Model particulars are given in [14] and presented in Table 1. According to "Instructions for CFD-Based Method" [7], test number 3a-2 is considered. Carriage velocity is fixed at $U_C = 1.531$ m/s, resulting in Froude number: $F_n = 0.28$ and Reynolds number: $R_n = 4.4643 \times 10^6$. Sway motion is defined with the amplitude: $\eta_0 = 0.317$ m, and number of PMM rotations per minute: $N = 8.021$ rpm.

Table 1: DTMB 5415 model particulars.

$L_{PP} =$	3.048 m
$B =$	0.410 m
$T =$	0.136 m
$\nabla =$	0.086 m^3
$m =$	83.35 kg

Mesh consists of 1 547 808 hexahedral and 89 610 polyhedral cells. The coordinate system is the one normally used for manoeuvring: right-handed with X positive forward, Y positive starboard and Z positive down. Origin is located at the intersection of still water line, centre line and mid-ship section. Mesh extends from 7.6 to -13.7 m in X direction, from 7.6 to -7.6 m in Y direction and 4.6 to -1.5 m in Z direction. Average mesh non-orthogonality is 9.5° while the maximum value is 88°.

Time step is varied automatically during the simulation based on the specified maximum CFL number of 50. However, average time step is around 0.009 s, giving approximately 800 time steps in one PMM period. Simulation time is approximately 90 hours for 5 PMM periods on Intel Core i5-3570K CPU at 3.4GHz with 15.6 GB memory (4 cores were used).

Simulation results are presented in form of graphs. Fig. 1 depicts the dimensional sway force signal in one PMM period. Authors believe that irregularities in raw signal (black, continuous line) are caused by ventilation problems. Since the mesh is not sufficiently fine to capture entrapped air bubbles, their possible presence lowers void fraction in the areas of the hull that should be fully submerged. Ventilation problems along with the irregular force signal only occurred for this particular case, which leads to conclusion that this phenomena could be mesh related. To filter out those irregularities, Fourier Series representation was used as described in [14] for experimental data analysis.

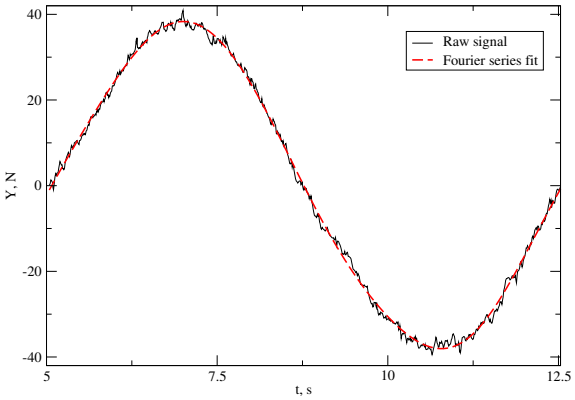

Figure 1: DTMB 5415 sway force signals: raw and Fourier series representation in one PMM period.

Fig. 2 presents the comparison of sway force over one PMM period with experimental results. Phase shift of the signal is obvious and it is believed to be related with ventilation problems since it is not present in the KCS simulation. Apart from the phase shift, CFD results tend to undershoot maximum values when compared to experiment by approximately 3% in troughs and 5% in crests.

Fig. 3 presents the dimensionless surge force compared with experimental results. Oscillations around mean values can be seen. CFD gives mean value of -0.02066 compared to experimental mean value of -0.01778. Relative error when compared to experiment is approximately 11%.

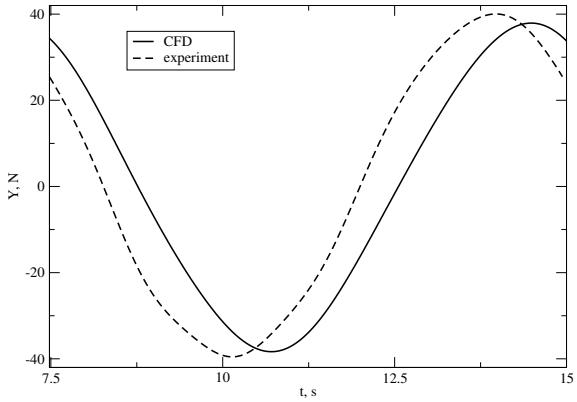

Figure 2: DTMB 5415 sway force comparison.

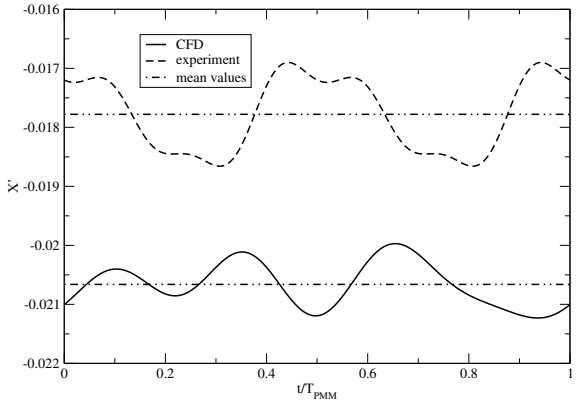

Figure 3: DTMB 5415 dimensionless surge force.

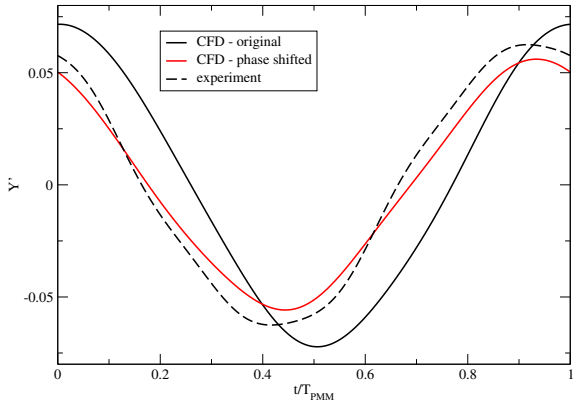

Figure 4: DTMB 5415 dimensionless sway force.

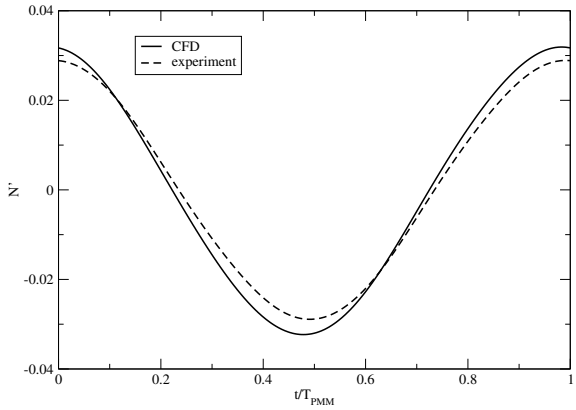

Figure 5: DTMB 5415 dimensionless yaw moment.

Using the least squares method, phase shift that minimises the error between CFD and experimental dimensionless sway force is found to be: $\delta\phi \approx 25°$ (or in time domain: $\delta T \approx 0.519$ s). Both original and phase shifted dimensionless sway forces are compared with experimental data in Fig. 4. The phase shift is again obvious but it is now accompanied with over prediction of maximum experimental values due to data reduction procedure that takes into account the motion of the ship, i.e. the sinusoidal $m\dot{v}_{PMM}$ term. On the other hand, this term causes a further reduction in the dimensionless amplitude for the phase shifted sway force. Corresponding maximum and minimum values for phase shifted sway force are undershot by approximately 10% when compared to experiment.

Fig. 5 compares dimensionless yaw moment with experimental data. In this case, maximum and minimum values of CFD are overshot by approximately 10% when compared to experimental results.

4.2 MOERI container ship - KCS

Pure sway motion of the MOERI container ship (KCS) with rudder is considered as a second test case. KCS particulars are presented in Table 2. According to "Instructions for CFD-Based Method" [7], test number 2a-4 is simulated. Even though the experimental results are obtained in a self-propulsion test, the propeller was not modelled in this approach. Carriage velocity is nearly constant at $U_C = 1.318$ m/s resulting in Froude number: $F_n = 0.202$ and Reynolds number: $R_n = 4.549 \times 10^6$. Sway motion is defined with the amplitude: $\eta_0 = 0.389$ m, and number of PMM rotations per minute: $N = 4.5$ rpm.

The computational mesh consists of 1 012 246 hexahedral, 3 500 tetrahedral and 83 492 polyhedral cells with 62 432 prisms. Wedges and pyramids are present in smaller number. The coordinate system is the one normally used for manoeuvring. Origin is located at the intersection of still water line and aft perpendicular. Mesh extends from 10.8 to -10.8 m in X direction,

Table 2: KCS model particulars. *Mass is calculated from density and displacement.

$L_{PP} =$	4.367 m
$B_{WL} =$	0.611 m
$T =$	0.205 m
$\nabla =$	0.356 m^3
$^*m =$	355.71 kg

from 10.8 to -10.8 m in Y direction and 10.8 to -5.4 m in Z direction. Average mesh non-orthogonality is 7.2° while the maximum value is 78°.
The first simulation was carried out with varying time step depending on the specified maximum CFL number of 500. Average time step is around 0.042 s, giving approximately 300 time steps in one PMM period. Simulation time was slightly below 10 hours for 5 PMM periods on Intel Core i7-4820K CPU at 3.7GHz with 15.6 GB memory (4 cores were used).
This test case was run with three different maximum CFL numbers: 500, 100 and 50. Fig. 6 presents raw sway force signals over one PMM period. Graph shows good agreement between these runs, leading to conclusion that the increase of time step by order of magnitude does not affect the results significantly. The same phenomena is observed for surge force and yaw moment but they are not presented here.

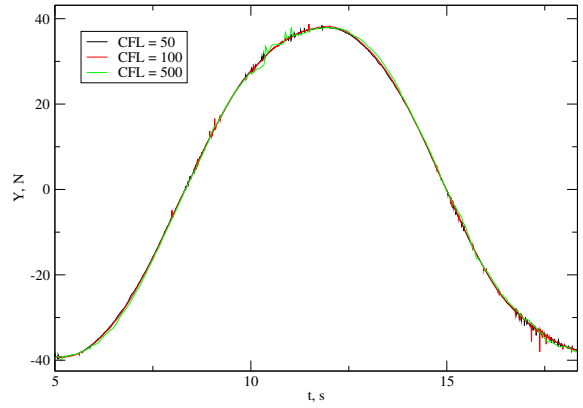

Figure 6: KCS sway force comparison for different maximum CFL numbers.

Data reduction is performed only for the $CFL_{max} =$ 100 run. When compared to experimental data, no phase shift between both sway force and yaw moment is present. Fourier series representation is again used in order to simplify the post-processing. Fig. 7 presents dimensionless surge force compared to experimental data. Mean CFD value is undershot by approximately 12.5%. Experimental surge force has larger oscillations around the mean value over one PMM period. Probable cause is the self-propulsion test, whereas present CFD model does not include propeller modelling, it is "towed" with constant velocity without the propeller.

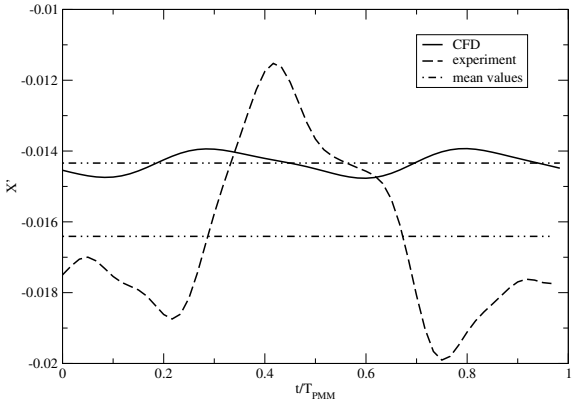

Figure 7: KCS dimensionless surge force.

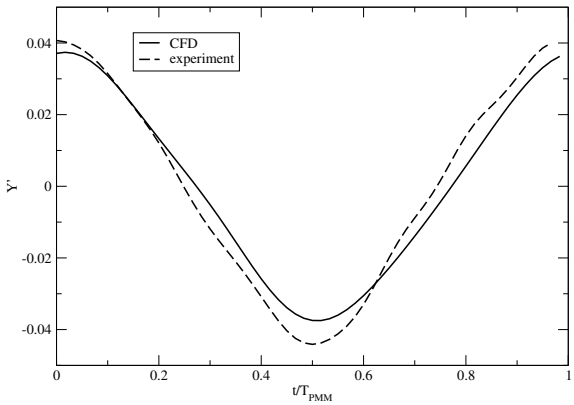

Figure 8: KCS dimensionless sway force.

Fig. 8 shows dimensionless sway force comparison. In contrast to DTMB, maximum and minimum values are undershot by approximately 8% and 15% respectively.
Fig. 9 presents dimensionless yaw moment compared to experimental data. In this case maximum and minimum values are overshot with CFD simulation by approximately 22% and 10%, respectively.

5 CONCLUSION

This work presented FVM simulations of pure sway manoeuvres. Both implicit treatment of all governing equations and novel formulation of compressive flux in the VOF equation extends the CFL number limit.

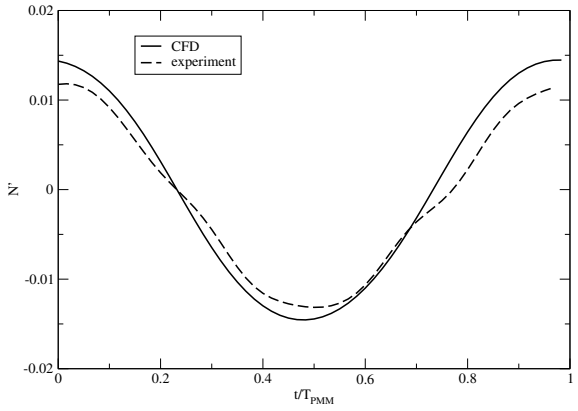

Figure 9: KCS dimensionless yaw force.

Maximum CFL numbers ranged from 50 to 500 for simulations carried out in this work.

Accuracy of the results was assessed on DTMB 5415 and KCS hull geometries. Sway force for the DTMB signal is phase shifted when compared to experimental results by approximately 7% of PMM period. This behaviour is not present for the yaw moment and generally for all forces/moments in KCS simulations. This leads to the conclusion that phase shift phenomena could be mesh related. Average surge force is over predicted in the DTMB case, whereas for the KCS case, it is under predicted. Peaks of sway forces and yaw moments are generally within 10 to 15% percent when compared to experimental data.

Time refinement study was carried out for the KCS case, where the maximum CFL number is varied from 50 to 500. It is shown that increase of time step by one order of magnitude does not affect the results significantly.

References

[1] J.U. Brackbill, D.B. Kothe, and C. Zemach. A continuum method for modelling surface tension. *J. Comput. Phys.*, 100:335–354, 1992.

[2] I. Demiridžić and M Perić. Space conservation law in finite volume calculations of fluid flow. *Int. J. Numer. Meth. Fluids*, 8:1037–1050, 1998.

[3] J. H. Ferziger and M. Peric. *Computational Methods for Fluid Dynamics*. Springer, 1996.

[4] H. Jasak. *Error Analysis and Estimation for the Finite Volume Method with Applications to Fluid Flows*. PhD thesis, Imperial College of Science, Technology & Medicine, London, 1996.

[5] H. Jasak, V. Vukčević, and D. Christ. Rapid Free Surface Simulation for Steady-State Hull Resistance with FVM using OpenFOAM. *30^{th} Symposium on Naval Hydrodynamics, Hobart, Tasmania, Australia, 2-7 November 2014*, 2014.

[6] L. Larsson, F. Stern, and M. Visonneau. *Numerical Ship Hydrodynamics: An assessment of the Gothenburh 2010 Workhop*. Springer, 2014.

[7] FORCE Technology Maritime Division. SIMMAN 2014: Workshop on Verification and Validation of Ship Manoeuvring Simulation Methods. `http://www.simman2014.dk`, 2014. [Online; accessed 26 September 2014].

[8] F. R. Menter. Two-Equation Eddy-Viscosity Turbulence Models for Engineering Applications. *AIAA Journal*, 32(8):1598–1605, 1994.

[9] F. R. Menter, M. Kuntz, and R. Langtry. Ten Years of Industrial Experience with the SST Turbulence Model. *Turbulence, Heat and Mass Transfer*, 4:625–632, 2003.

[10] H. Rusche. *Computational Fluid Dynamics of Dispersed Two - Phase Flows at High Phase Fractions*. PhD thesis, Imperial College of Science, Technology & Medicine, London, 2002.

[11] O. Ubbink and R. I. Issa. A method for capturing sharp fluid interfaces on arbitrary meshes. *Journal of Computational Physics*, 153:26–50, 1999.

[12] B. van Leer. Towards the Ultimate Conservative Difference Scheme. IV. A New Approach to Numerical Convection. *Journal of Computational Physics*, 23:276–299, 1977.

[13] H. G. Weller, Tabor. G., and H. Jasak. A tensorial approach to computational continuum mechanics using object oriented techniques. *Computers in Physics*, 12:620–631, 1998.

[14] H. Yoon, C. Simonsen, L. Benedetti, J. Longo, Y. Toda, and F. Stern. Benchmark CFD Validation Data for Surface Combatant 5415 in PMM Maneuvers - Part I: Force/Moment/Motion Measurements. *Ocean Engineering (submitted)*, 2014.